Ultramicroscopy 45 (1992) 145–154
North-Holland

ultramicroscopy

Registry and UHV transmission electron diffraction of surfaces

L.D. Marks
Department of Materials Science, Northwestern University, Evanston, IL 60208, USA

Received 2 March 1992

A model using a distorted wave analysis coupled with considerations of registry and channeling is developed for understanding high-energy electron diffraction from surfaces in a plan-view geometry. We show that this model explains strong effects due to inelastic scattering, particularly for the 1×1 surface spots as a function of beam orientation with respect to the underlying bulk substrate and with respect to the effect of registry on intensities. Numerical simulations using the multislice algorithm are correlated with the model, and show additional complications due to a top–bottom effect and coupling.

1. Introduction

Exploration of the character of high-energy (100–300 kV) electron diffraction of surfaces in a plan-view geometry where the beam is normal to the surface of interest is a relatively recent development. The motivation for this has been the development of microscopes which can operate in the ultra-high vacuum (UHV) required for control of surface chemistry to a level where the results are meaningful. Much of the theoretical study to date, e.g. refs. [1–6], has concentrated on relatively weak diffraction phenomena and understanding or verifying that diffraction patterns could be interpreted with a kinematical model. Somewhat more comprehensive are three Bloch-wave analyses [4–6] which have performed limited explorations of the effects of beam orientation, whether the reconstruction is on the top or bottom surface and dynamical diffraction effects. The driving force for this theoretical effort was the interpretation of the Si(111) 7×7 reconstruction by transmission electron diffraction [7,8], and experimental results using relatively weak diffraction from very thin samples, e.g. [9,10].

In our own work on surfaces [11–13] we have observed that it was easy to obtain images of surfaces under conditions where there was strong diffraction from the bulk of the sample, i.e. near to a zone-axis orientation. This raises the question of understanding such images. Obviously the geometry of such a diffraction pattern will be similar to a standard double-diffraction pattern, but what about the intensities? In principle, electron diffraction at these energies is a very mature topic, so any information can be simulated by a forward calculation based upon some hypothetical structure, with few to no adjustable parameters in the diffraction calculation. However, this can only be done in a forward fashion, and one cannot invert such complicated calculations but only use them in a trial-and-error fashion to fit the experimental results.

This introduces a subtle but critical problem. Electron microscopy under UHV conditions has to be done fairly fast, since even in 10^{-10} Torr surfaces contaminate. There are so many different experiments that can be done within a modern electron microscope by a push of a button that it is easy to lose the trees in the woods. To put this in perspective, arguably the most useful model in electron microscopy is the two-beam approximation [14]. The reason that this is so powerful is not that it is rigorously correct, but rather that it has a simple closed-form solution, includes most of the relevant effects and can

therefore guide the researcher sitting at the microscope to interpret images as they appear on the phosphor screen. Models of this type are needed for UHV microscopy of surfaces since one cannot afford to analyze the data for a few days and then go back and collect more information from the same area.

The purpose of this note is to try to develop a model of this character. It is shown that a distorted wave analysis (DWA) using Bloch waves qualitatively describes many of the trends found in numerical computer calculations of surface diffraction. Of particular significance, we show that the registry of a surface reconstruction has a very substantial effect on the resultant diffraction intensities, as does the top-bottom effect and coupling. We should note that the background to this work was first the numerical calculations and then, at a later stage, the model was developed to explain the calculation results, although we will present the data in the opposite order. We will focus here only on the diffraction; high-resolution imaging of surfaces in a plan-view geometry will be dealt with in a separate paper.

2. Theoretical model

To cleanly define the issues, let us first consider a conventional kinematical analysis for a surface forbidden spot and examine the approximations that it requires. We will consider, explicitly, a (110) diffraction spot for an fcc lattice with a systematic orientation near to a [001] zone. For reference, the Ewald sphere of relevance is shown in fig. 1. Taking just the incident beam into account, the amplitude of the (110) spot, ϕ_g, with a kinematical approximation is:

$$\phi_g = \sin(\pi t s_z)\, \exp(\pi i t s_z) \sum_n (\pi i/\xi_h) \Big/ \pi[s_z + nv], \tag{1}$$

where $\boldsymbol{h}$ and $\boldsymbol{v}$ are the reciprocal lattice vectors (1, 1, $n+1$) and (002) respectively, t the thickness and ξ_h the extinction distance. (In normal diffraction s_z is small, so the summation can be truncated with only the $n = 0$ term; but this appears to be dubious if s_z is large.)

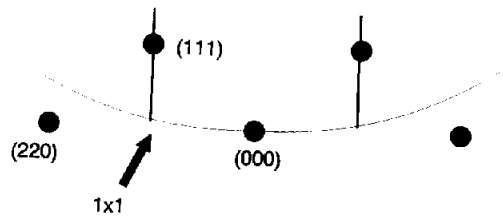

Fig. 1. Illustration of the Ewald sphere issue with 1×1 spots on a (001) zone axis. The 1×1 spots are due to the $(11n)$ spots, and for the two shown they are in the Bragg condition for the (220) reflections. With the other dimension included, they are also in the Bragg condition for (200) and (020) reflections.

The (kinematical) wave is then:

$$\psi(\boldsymbol{r}) = \left\{1 + \phi_g \exp(2\pi i \boldsymbol{g}\cdot\boldsymbol{r})\right\} \exp(2\pi i \boldsymbol{k}\cdot\boldsymbol{r}), \tag{2}$$

where $\boldsymbol{k}$ is the incident wavevector.

Two conditions are required for eqs. (1) and (2) to be valid, namely:
(a) ϕ_g must be small, so that the attenuation of the transmitted beam is small enough to ignore;
(b) $\exp(2\pi i[\boldsymbol{k}+\boldsymbol{g}]\cdot\boldsymbol{r})$ is a valid solution for an electron in the crystal.

The critical point about surface diffraction in transmission is that (a) above should almost always be valid, but (b) may well be invalid; numerical simulations (see below) and energy-filtered experimental measurements [15] indicate that $\phi_g \approx 0.02$. To illustrate this most clearly, for the systematic condition shown in fig. 1 (110) and $(\bar{1}\bar{1}0)$ are in fact at the exact Bragg condition with respect to each other for a (220) diffraction process and are therefore very strongly coupled together.

The appropriate method to use in general is therefore to consider the scattered waves arising from the surface in terms of stationary solutions for the bulk crystal. With the assumption that the additional potential of interest (perturbation) is small, we can use the distorted wave approximation; this approach appears to be standard in electron diffraction theory. To be a little more specific, let $U(\boldsymbol{r})$ be the (small) potential due to

the surface scattering, here the higher-order Laue ($11n$) potential terms. In the absence of these, we can write the electron wave as a sum of (normalized) Bloch waves $\exp(2\pi i \boldsymbol{k}_j \cdot \boldsymbol{r}) b_j(\boldsymbol{r}, \boldsymbol{k}_j)$:

$$\psi_0(\boldsymbol{r}) = \sum_j \alpha_j \exp(2\pi i \boldsymbol{k}_j \cdot \boldsymbol{r}) b_j(\boldsymbol{r}, \boldsymbol{k}_j). \quad (3)$$

If $\exp(2\pi i[\boldsymbol{k}_l + \boldsymbol{g}] \cdot \boldsymbol{r}) b_l(\boldsymbol{r}, \boldsymbol{k}_l + \boldsymbol{g})$ is a (normalized) Bloch wave displaced by $\boldsymbol{g} = (110)$, the amplitude of this Bloch wave is:

$$\beta_l = \int \exp(-2\pi i[\boldsymbol{k}_l + \boldsymbol{g}] \cdot \boldsymbol{r}) b_l^*(\boldsymbol{r}, \boldsymbol{k}_l + \boldsymbol{g}) U(\boldsymbol{r}) \times \psi_0(\boldsymbol{r})\, d\boldsymbol{r}, \quad (4)$$

with the full wave:

$$\psi(\boldsymbol{r}) = \psi_0(\boldsymbol{r}) + \sum_l \beta_l \exp(2\pi i[\boldsymbol{k}_l + \boldsymbol{g}] \cdot \boldsymbol{r}) \times b_l(\boldsymbol{r}, \boldsymbol{k}_l + \boldsymbol{g}). \quad (5)$$

Eq. (5) is a distorted wave analysis to first order in β_l, and will be valid so long as this term is small. Since the intensities of surface diffraction spots in transmission are of the order of 10^{-4} of the transmitted beam intensities, this should be valid in almost all cases.

Going from the simple form of the kinematical eq. (2) to include the bulk diffraction in eq. (5) can have a massive effect. To demonstrate this, we will show here that eq. (5) predicts very strong inelastic attenuation of the surface spots on a zone axis. Considering the systematic condition in fig. 1, there are two possible Bloch waves just using (110) and $(\bar{1}\bar{1}0)$, $\cos(2\pi \boldsymbol{g} \cdot \boldsymbol{r})$ and $\sin(2\pi \boldsymbol{g} \cdot \boldsymbol{r})$, where $\boldsymbol{g} = (110)$ as above. Taking just the (220) and $(\bar{2}\bar{2}0)$ bulk spots, only two Bloch waves can be excited in the bulk crystal, i.e.

$$b_1(\boldsymbol{r}, \boldsymbol{k}_1) = \exp(2\pi i \boldsymbol{k}_1 \cdot \boldsymbol{r})\{1 + \epsilon \cos(4\pi \boldsymbol{g} \cdot \boldsymbol{r})\},$$
$$b_2(\boldsymbol{r}, \boldsymbol{k}_2) = \exp(2\pi i \boldsymbol{k}_2 \cdot \boldsymbol{r})\{1 - \epsilon \cos(4\pi \boldsymbol{g} \cdot \boldsymbol{r})\}, \quad (6)$$

where the exact value of ϵ depends upon the crystal potential, but is not so important here. Since $U(\boldsymbol{r})$ has the form $U_g \cos(2\pi \boldsymbol{g} \cdot \boldsymbol{r}) \exp(2\pi i s_z z)$, the coupling to Bloch wave 1 ($b_1(\boldsymbol{r}, \boldsymbol{k}_1)$) is of order $U_g/2\{1 + \epsilon/2\}$, and to Bloch wave 2 of order $U_g/2\{1 - \epsilon/2\}$, and only the Bloch wave $\cos(2\pi \boldsymbol{g} \cdot \boldsymbol{r})$ is excited. Noting that Bloch wave 1 will suffer far more from inelastic scattering since it has maxima at the atomic positions, as will the Bloch wave $\cos(2\pi \boldsymbol{g} \cdot \boldsymbol{r})$, we have an immediate prediction of strong absorption.

From this simplified argument, a substantial number of effects due to inelastic scattering follow almost immediately. For instance, for a reconstruction on the top surface of a sample and the beam normal to this, the Bloch wave coefficients are:

$$\beta_l = \int \exp(-2\pi i[\boldsymbol{k}_l + \boldsymbol{g}] \cdot \boldsymbol{\rho}) b_l^*(\boldsymbol{r}, \boldsymbol{k}_l + \boldsymbol{g}) \times U(\boldsymbol{\rho})\, d\boldsymbol{\rho}, \quad (7)$$

where $\boldsymbol{\rho}$ is in the plane of the surface. Dependent upon the registry, symmetry and periodicities of the surface layer these Bloch waves may channel [16–18] either between the atoms or through them. For instance, if the surface atoms are in registry with respect to the bulk, the bulk waves excited are those which "see" the crystal potential most strongly. Therefore there will be strong inelastic attenuation and also dynamical diffraction. In addition the variation with tilt will be slow; the more strongly bound Bloch waves have flatter dispersion surfaces and therefore disperse more slowly. When the atoms are not in registry, the bulk waves excited are the weakly bound ones for which there is less inelastic scattering and diffraction. Furthermore, the dependence upon the beam orientation with respect to the crystal will be faster since these levels are more dispersive.

The final concept that needs to be mentioned is coupling. This concept was first considered by Peng and Whelan [4], who considered whether it was possible to "couple" two different surface waves by a bulk diffraction vector as their definition. From the analysis above, the more critical question is whether two or more diffracted beams combine to give large or small intensities at the atomic sites of a reconstruction for a given thickness. We will use this definition since registry, as shown with explicit calculations below, is the major issue.

In the following section, we will present multislice results which demonstrate a number of features, in particular about the role of inelastic scattering registry and top–bottom effects for surfaces.

3. Numerical method

Multislice calculations for the very large unit cells often found in reconstructed surfaces are technically difficult, and unless care is taken can

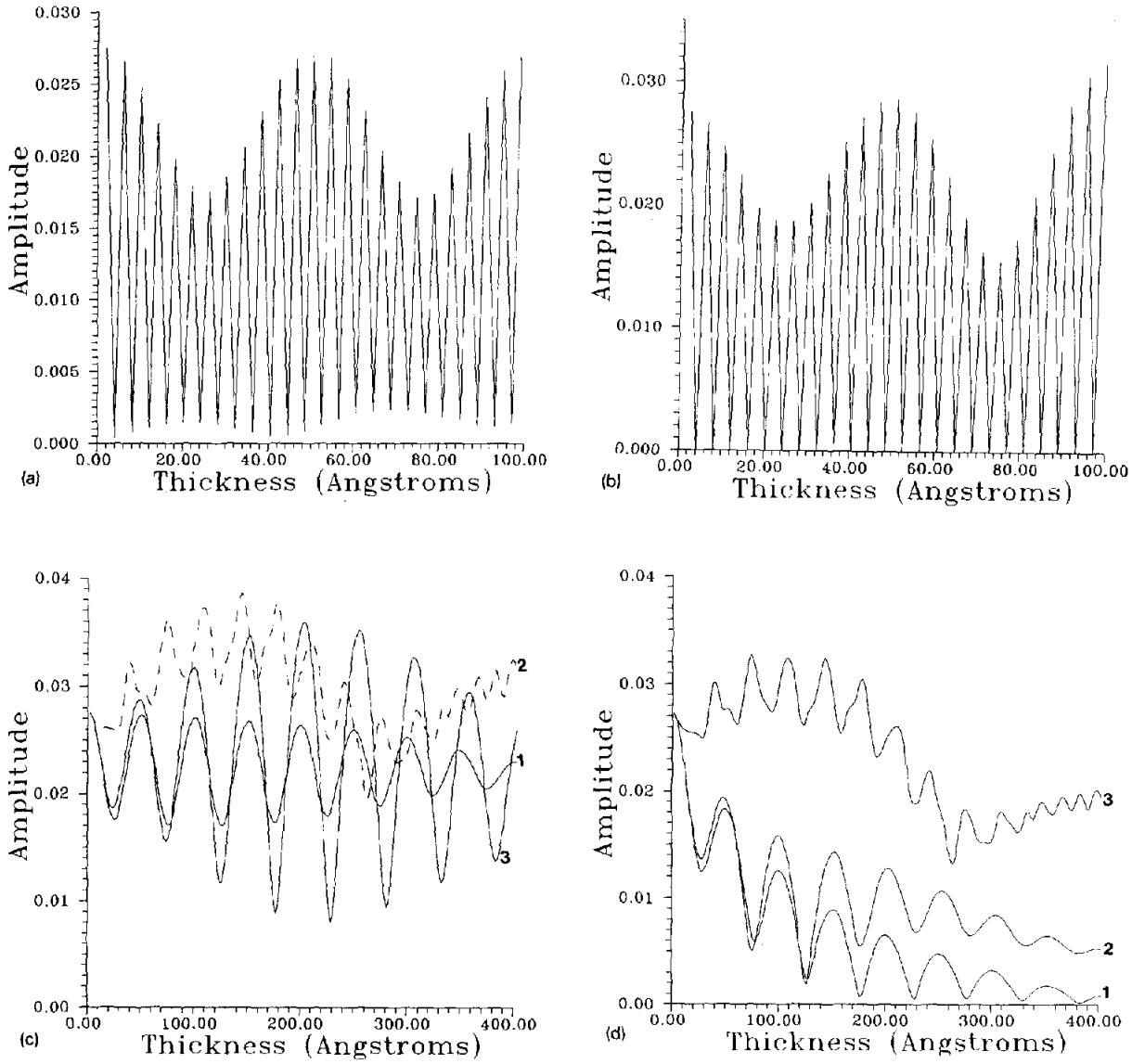

Fig. 2. Amplitude of the (110) or (01) spots for various cases: (a) on the zone showing the odd/even slice oscillations with no inelastics; (b) tilted to bring the (110) beam to the Bragg condition with no inelastics; (c) the three cases as indicated in the text without inelastic scattering; (d) with inelastic scattering and (e) the ratio 2c/2d scaled by the transmitted intensities. In (e) the peaks in the ratio for case 2 at thicknesses of about 23 and 30 nm are misleading (in the ratio approach) and are caused by a small shift of the oscillation frequency with inelastic scattering.

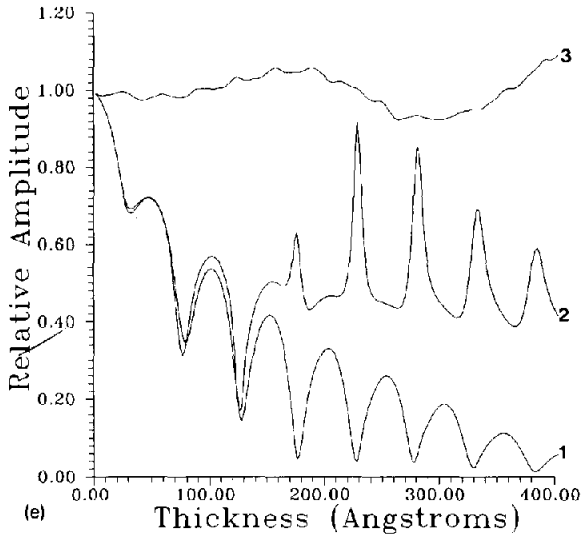

Fig. 2 (continued).

be erroneous [19]. For reference, we will briefly detail the approach used.

All the calculations were performed using the NUMIS software developed by the author, using the standard multislice algorithm [20–22]. To ensure convergence of the calculations, the simulations were all performed with a reciprocal space sampling to at least 40 nm^{-1}, and typical slice thicknesses of < 0.2 nm; these are critical for calculations that extend beyond very thin (< 5 nm) crystals. Inelastic scattering was simulated by including an imaginary component to the potential of 0.05 or 0.075. We will not claim that this is accurate, but it should demonstrate the type of effects to be found; more work needs to be done on how to include inelastic scattering within multislice.

With a standard multislice program it is easy to simulate with the reconstruction on the top surface, very tedious to simulate different thicknesses with it on the bottom surface. A slightly modified version of the code was written to store the wave through the crystal temporarily, incorporate the phase gratings for a bottom surface reconstruction, and then retrieve the perfect crystal wave. This permitted bottom surface simulations to be rapidly performed as a function of thickness.

It should be noted that we are only including here a limited number of results; more calculations have been performed and this note is a condensed version of the highlights. We will also use throughout surface mesh axis for the 1×1 surface to index reconstruction spots.

4. Numerical results

We will first focus on the "1×1" diffraction process, strictly speaking a higher-order Laue zone scattering process, since these are often the strongest surface spots in a pattern.

4.1. 1×1 diffraction

The key results are shown in fig. 2, plots of the intensity of the 1×1 spots as a function of thickness with and without inelastic scattering for three conditions: (1) exactly on the zone axis, (2) with a small tilt off the zone axis to put a 1×1 in the Bragg condition and (3) with a large, additional tilt normal to this. Excepting figs. 2a and 2b only the data from odd slices is shown; for an even number of slices the intensity is small to zero. All the simulations are for a gold (001) zone, focusing on the (110) spots, with an accelerating voltage of 300 kV.

On the zone axis, there is a strong attenuation of the 1×1 spots when inelastic scattering is included. (Experimental problems in imaging with the 1×1 spots near to a zone axis were mentioned by Levitt and Howie [24], although no explanation was offered.) There are also some oscillations in the intensity, which have two origins. First, going back to the DWA discussion, the 1×1 spots are, strictly speaking, Bloch waves. As such, they will show the same sort of oscillatory intensity with thickness of any diffraction process, as mentioned previously by Lynch [23] and Levitt and Howie [24]. Secondly, the excitation error for these spots is not exactly one over the planar spacing along the beam direction, so there will be some additional modulation by this term [25]. We should note that for this case the amplitude for an even number of slices was not, in general, zero.

In case (2), the thickness dependence is somewhat simpler. Here the excitation error is exactly one over the planar spacing, so the modulation has a simple "high-frequency" component along the lines of the total number of planes in the crystal as discussed by Cherns [26]; for even numbers of slices the amplitude is exactly zero. Note, however, that the inelastic component has a major effect in damping the intensity.

Finally, for case (3) we can see that the inelastic effect has been substantially reduced. The 1×1 diffraction no longer corresponds to a strongly channeled set of Bloch waves in the bulk material. (For even numbers of slices the intensity is identically zero.)

The trends are most clearly shown in fig. 2e, where it is apparent that off the zone axis the (110) amplitude is behaving essentially the same as the transmitted beam, whereas on the zone axis at the modest thickness of 40 nm it is attenuated by more than 90%.

4.2. Registry

The 1×1 diffraction clearly shows very strong effects due to inelastic scattering because the wave is strongly diffracted by the bulk lattice. What about a surface reconstruction on the top surface? We have to consider the registry of the surface layer with respect to the bulk, which turns out to be the dominant term. If the layer is in registry, one can predict very strong effects both in terms of dynamical diffraction of the layer when it is on the top surface and for inelastic scattering. To test this, multislice simulations were carried out for the two test "5×1" gold reconstructions shown in fig. 3. Of these two, one is in perfect registry with the bulk and the second exact non-registry. The results, shown in fig. 4, dramatically demonstrate the expected effects; for perfect registry strong dynamical scattering and inelastic attenuation are observed whereas for complete non-registry the effects are quite different.

To discuss this a little further, let us focus on some aspects of the results. Fig. 4a shows the ratio of the inelastic to elastic (1/5,1) amplitudes. For the unregistered case, the surface wave is being anomalously transmitted through the bulk, compared to anomalous adsorption with exact registry. It is important to mention that this ratio was not a function of incident angle as evidenced by rocking curve calculations (not shown) – the reason for mentioning this will become apparent below. Fig. 4b compares the amplitudes with inelastic scattering for the two cases on the zone with the reconstruction on the top or bottom surface. For the registered case, the amplitude is a weak function of whether the top or bottom surface is used; the relevant wave tracks through the atomic columns in both cases due to channeling. This is not the case for the unregistered case,

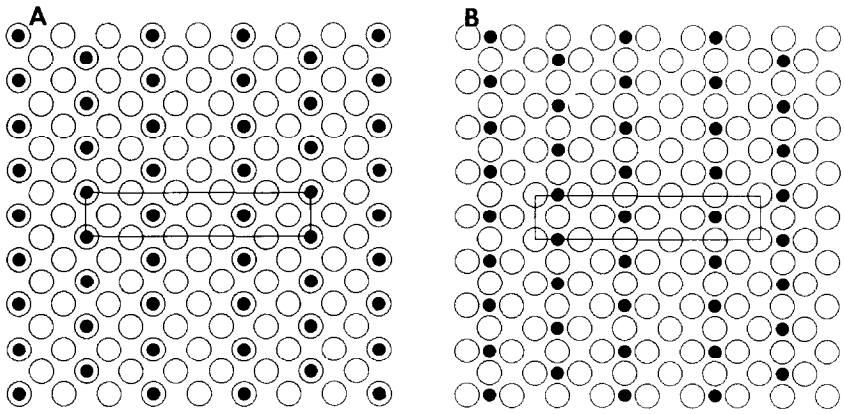

Fig. 3. Two fictitious gold (001) 5×1 reconstructions: (a) with complete registry and (b) without any registry.

since the amplitude outside of the atomic columns is not channeled. The role of channeling is perhaps clearer in fig. 4c which shows the variation with thickness with the reconstruction on top for three different tilts. The Bloch waves for the registered case are the strongly channeled, weakly dispersive (i.e. flat dispersion surface) levels with only a slow variation with tilt of the diffraction; the unregistered, weakly bound and dispersive waves change faster with tilt.

4.3. Surface reconstruction

In order to illustrate what is going on for the case of a surface reconstruction, we have chosen to consider a 5×1 (001) reconstruction for gold

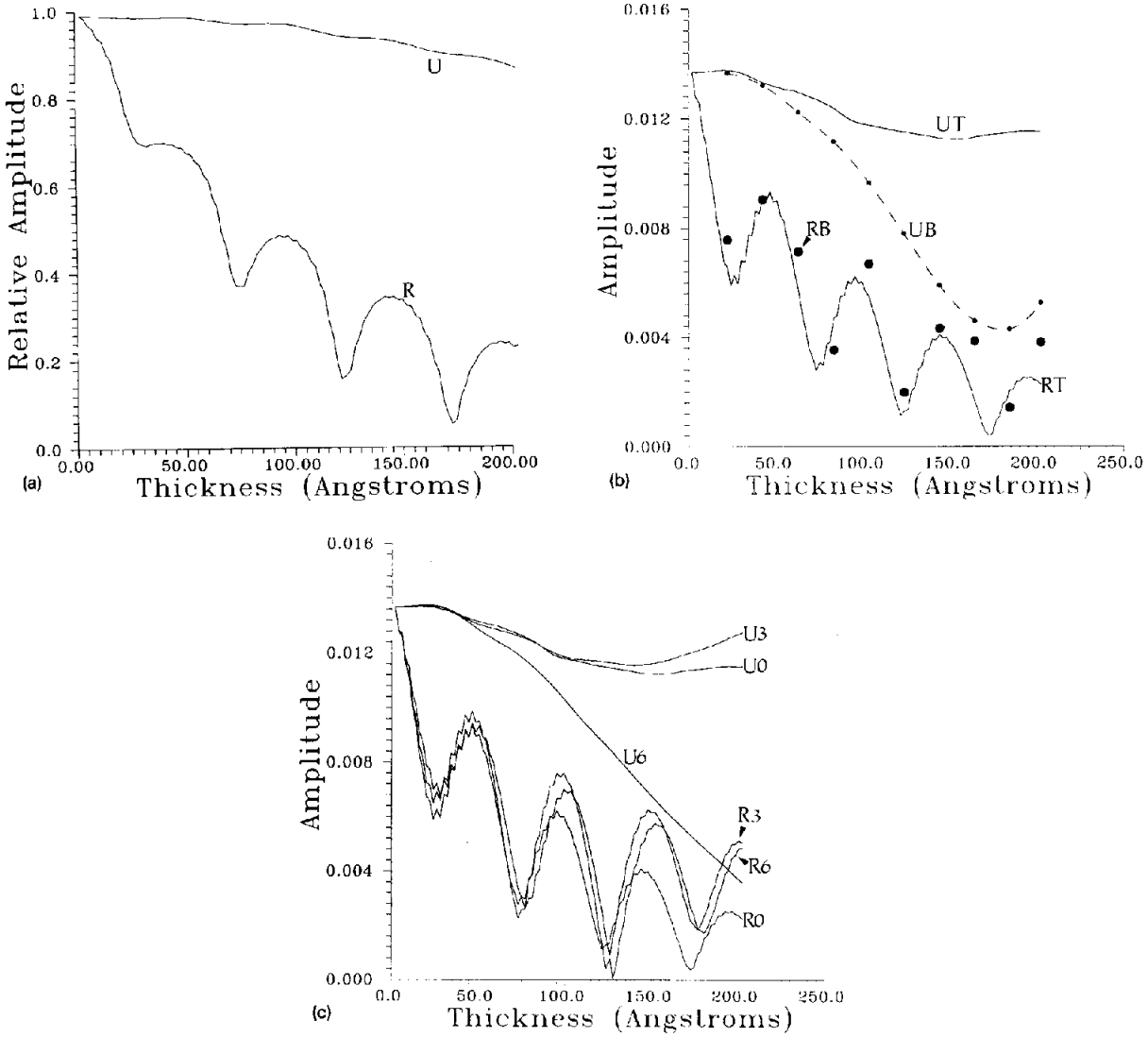

Fig. 4. Amplitudes for the two models in fig. 3, "U" marking the unregistered case and "R" the registered case all for the (1/5,1) spot: (a) comparison of the ratio of the inelastic, note the dramatic drop in the registered case; (b) thickness variation with the reconstruction on the top surfaces (lines, UT and RT) and bottom surface (circles and dashed line, UB and RB); (c) variation with tilts of 0, 3 and 6 mrad for the top surface in both cases marked Rn and Un with $n = 0$, 3 and 6.

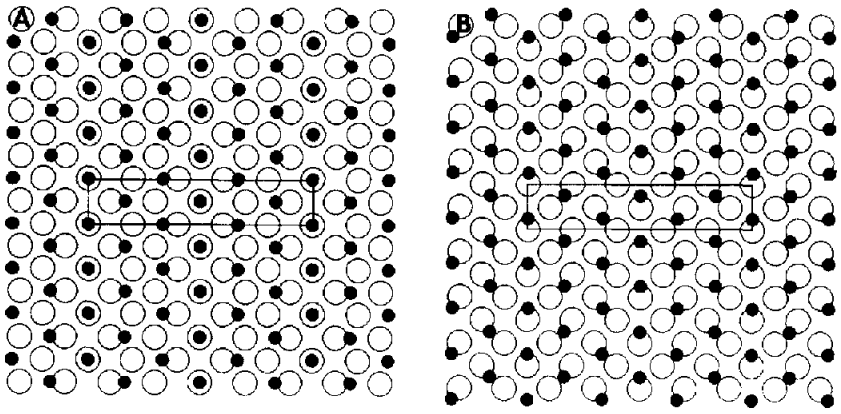

Fig. 5. Two versions of a hypothetical gold (001) 5×1 reconstruction with partial registry in (a) and with a small shift to low registry in (b).

and examine two possible registries as shown in fig. 5. The first has the hexagonal gold overlayer exactly over the underlying gold (001) bulk, the second slightly off. Shown in figs. 6 and 7 are rocking curves of the (3/5,1) spot for a thickness of 20 nm (100 slices) for the two types of reconstruction on the top and bottom surfaces and with and without inelastic scattering.

There is a disturbing amount of variation in the amplitudes in these figures, but some points can still be made. First, inelastic scattering has a stronger effect for the more registered reconstruction, particularly when it is on the bottom surfaces, although the negative tilt region in fig. 6a shows that this is a weak generalization. (This is presumably because the reconstruction is at least partially unregistered in both cases.) Second, there is a maximum for positive tilt for the registered case, and a minimum for the non-registered case at tilts of about 5.0 mrad with the

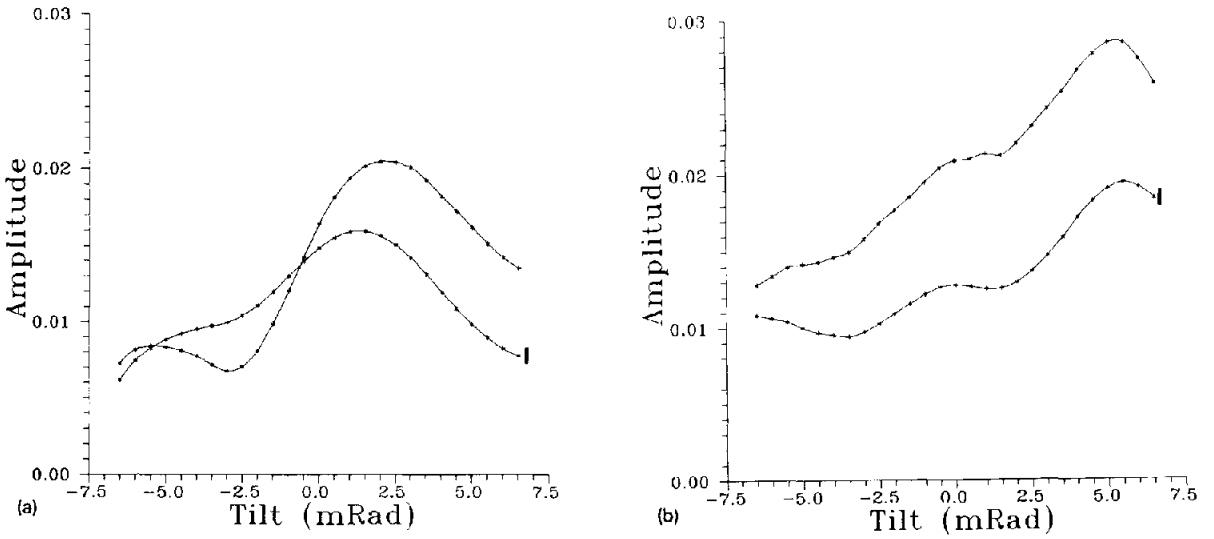

Fig. 6. Comparisons of the (3/5,1) spot amplitude as a function of beam tilt with a thickness of 20 nm for the structure in fig. 5a: (a) with the reconstruction on the top surface and (b) with it on the bottom surface. For both, the rocking curves with inelastic scattering are marked "I".

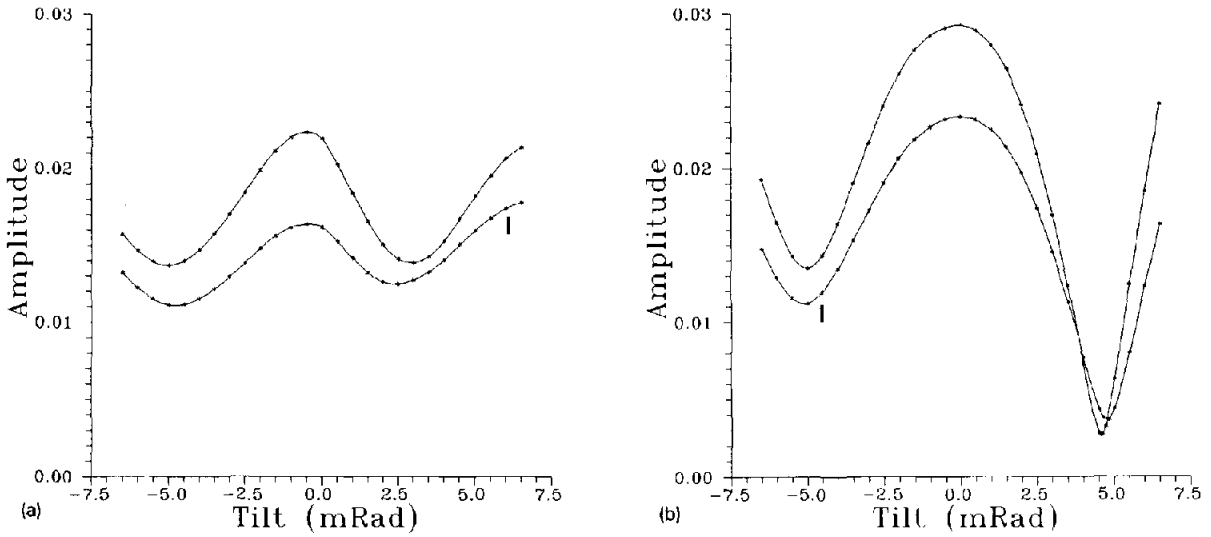

Fig. 7. Comparisons of the (3/5,1) spot amplitude as a function of beam tilt with a thickness of 20 nm for the structure in fig. 5b: (a) with the reconstruction on the top surface and (b) with it on the bottom surface. The strong minimum about 4.5 mrad positive is due to the destructive interference of scattering from the (000) and (220) bulk spots. The minimum is non-zero (there are additional calculation points to confirm this), but is a factor of 100 lower, so will be near zero in an experimental diffraction pattern. For both, the rocking curves with inelastic scattering are marked "I".

reconstruction on the bottom surface. This is due to strong coupling; at the thickness chosen for these tilts the amplitudes of the (00) and (02) spots (bulk (000) and (220)) are equal. For the unregistered case this leads to destructive interference, constructive interference for the registered case. The final point is that the intensity of the reconstruction on the bottom surface tends to be stronger than that on the top surface, but not in all cases.

5. Discussion

We have attempted herein to develop a simple model to assist interpretation of the diffraction processes in plan-view imaging under strong diffraction conditions. The model seems to work well, and gives a very direct interpretation of the critical nature of inelastic scattering from surfaces and the role of registry. As mentioned in an earlier note [19], these effects are unusually strong; inelastic scattering at the thicknesses used in this paper is normally considered to be a small effect. The key point in understanding this appears to be the relationship between the symmetry and spatial location of the surface-sensitive waves relative to the bulk atomic positions.

When this work was started, it was hoped to find a simple methodology of interpreting surface intensities as mentioned in the introduction. The 1×1 spots are quite simple to interpret, and also do not appear to be true surface-sensitive features. Unfortunately, nothing else seems to be very simple, and it looks like interpreting information with strong diffraction conditions may well require extensive computer simulations. Full interpretation is going to require levels of rigor comparable to those needed for a good structure determination from HREM, for instance matching *several* diffraction patterns (or images) as a function of thickness and orientation. The destructive resonance in fig. 7b may be exploitable in some cases if one can arrange to have the reconstruction on only one surface, which can (sometimes) be done experimentally; we hope to try this in the near future.

A few comments are appropriate about inelastic scattering, which is clearly going to be an issue. An imaginary component of the potential

may include the attenuation of the diffracted beams, so it might be possible to use such calculations to match energy-filtered diffraction patterns. Unfortunately, for imaging the issue is more complicated. Experimental measurements [15] indicate that the diffuse plume around the strong diffraction spots (for silicon) is due to plasmon scattering. Higher-resolution imaging modes will include these, and there will be both chromatic and convergence effects. There is also the issue of the coherence of the plasmons; plasmon losses of different energies are mutually incoherent, but it would be dangerous and possibly incorrect to assume that losses of a given energy are incoherent for different scattering angles. It would be extremely informative to obtain and then attempt to match through-thickness, through-focus plasmon loss images in a STEM for moderate-thickness samples in order to measure the coherence or incoherence.

As a final comment, it is appropriate to consider the conclusions from this work relative to earlier analyses [1–6] of the character of surface diffraction from reconstructed surfaces. First, it is clear that the diffraction is not kinematic, as has now been demonstrated experimentally [3]. Second, we should also point out that it is easy to get such calculations wrong; for instance, the slow convergence of the sum in eq. (1) will be problematic for Bloch wave approaches, but seems to be implicitly included in standard multislice calculations [19]. With respect to the earlier Bloch wave analyses [4–6], these all appear to be correct, but the whole situation is sufficiently complicated with at least four (coupling, registry, top versus bottom surface, inelastic scattering) simultaneous phenomena that there is more to the full story. It would not come as a surprise to discover additional phenomena as more experimental and theoretical results become available. For instance, the strong destructive interference in fig. 7b was discovered purely by accident; if a smaller thickness had been chosen it would probably not have shown up for the range of tilts used.

Acknowledgement

The author would like to acknowledge support from the Air Force Office of Scientific Research on grant number AFOSR 86-0344 DEF.

References

[1] J.C.H. Spence, Ultramicroscopy 11 (1983) 117.
[2] Y. Tanishiro and K. Takayanagi, Ultramicroscopy 27 (1989) 1.
[3] L.D. Marks, T.S. Savage, J.P. Zhang and R. Ai, Ultramicroscopy 34 (1991) 343.
[4] L.M. Peng and M.J. Whelan, Acta Cryst. A 47 (1991) 101.
[5] K. Nakai, Surf. Sci. 202 (1988) 99.
[6] K. Takayanagi, Acta Cryst. A 46 (1990) 83.
[7] K. Takayanagi, Y. Tanishiro, S. Takahashi and M. Takahashi, Surf. Sci. 164 (1985) 367.
[8] K. Takayanagi, Y. Tanishiro, M. Takahashi and S. Takahashi, J. Vac. Sci. Technol. A 3 (1985) 1502.
[9] K. Yamazaki, K. Takayanagi, Y. Tanishiro and K. Yagi, Surf. Sci. 199 (1988) 595.
[10] K. Takayanagi, Y. Tanishiro, K. Yagi, K. Kobayashi and G. Honjo, Surf. Sci. 205 (1988) 637.
[11] L.D. Marks, R. Ai, J.E. Bonevich, M.I. Buckett, D. Dunn, J.P. Zhang, M. Jacoby and P.C. Stair, Ultramicroscopy 27 (1991) 90.
[12] D.N. Dunn, R. Ai, T.S. Savage, J.P. Zhang and L.D. Marks, Ultramicroscopy 38 (1991) 333.
[13] J.E. Bonevich and L.D. Marks, Microscopy 22 (1992) 95.
[14] P. Hirsch, A. Howie, R.B. Nicholson, D.W. Pashley and M.J. Whelan, Electron Microscopy of Thin Crystals (Krieger, New York, 1977).
[15] P. Xu and L.D. Marks, Ultramicroscopy 45 (1992) 155.
[16] M.V. Berry, J. Phys. C4 (1971) 697.
[17] K. Kambe, G. Lehmpfuhl and F. Fujimoto, Z. Naturforsch. 29a (1974) 1034.
[18] A.M. Ozori de Almeida, Acta Cryst. A 31 (1973) 435.
[19] L.D. Marks, Ultramicroscopy 38 (1991) 325.
[20] J.M. Cowley and A.F. Moodie, Acta Cryst. 10 (1967) 609.
[21] P. Goodman and A.F. Moodie, Acta Cryst. A 30 (1974) 280.
[22] P.G. Self, M.A. O'Keefe, P.R. Busek and A.E.C. Spargo, Ultramicroscopy 11 (1983) 35.
[23] D.F. Lynch, Acta Cryst. A 27 (1971) 399.
[24] J.P.F. Levitt and A. Howie, J. Microscopy 116 (1979) 89.
[25] J.M. Gibson, private communication, 1991.
[26] D. Cherns, Phil. Mag. 30 (1974) 549.